Efficient Resonant Drive of Flapping-Wing Robots

Stanley S. Baek, Kevin Y. Ma, and Ronald S. Fearing

Abstract— **Flapping-wing air vehicles can improve efficiency by running at resonance to reduce inertial costs of accelerating and decelerating the wings. For battery-powered, DC motor-driven systems with gears and cranks, the drive torque and velocity is a complicated function of battery voltage. Hence, resonant behavior is not as well defined as for flapping-wing systems with elastic actuators. In this paper, we analyze a resonant drive to reduce average battery power consumption for DC motor-driven flapping-wing robots. We derive a nondimensionalized analysis of the generic class of a motor-driven slider crank, considering motor and battery resistance. This analysis is used to demonstrate the benefits of efficient resonant drive on a 5.8g flapping-wing robot and experiments showed a 30% average power reduction by integrating a tuned compliant element.**

I. INTRODUCTION

Flapping-wing flight in nature has unparalleled maneuverability, agility, and hovering capability. Over the last few decades, engineers have made remarkable progress toward the design of flapping-wing micro air-vehicles (MAVs) inspired by biological systems. However, a recurring issue in the development of effective MAVs is that small-scale flapping-wing robots require substantial amounts of power to generate lift. MAVs use portable power sources with limited energy capacity. This paper calculates the time average power used by a flapping wing MAV with a constant voltage drive, including battery and motor resistance. Previous work in resonant drive of flapping wing MAVs has considered minimizing input power assuming constant velocity [19]. However, for heavily loaded structures, motor velocity will not be constant without a speed controller, which takes active power for deceleration. Another related result considers minimizing peak torque [12], [14], which improves motor sizing, yet does not consider the effects of the battery resistance. We show that under certain loading conditions, the battery and motor resistance will influence the time average power required.

Efficient power usage is fundamental to the development of flapping-wing MAVs. One approach to this objective is to use integrated compliant mechanisms driven at their resonant frequency. Goldfarb developed piezoelectric-actuated flapping-wing MAVs excited at the resonant frequency [3],

[6], [13]. Agrawal demonstrated a novel, motor-driven four-bar crank-rocker mechanism that integrated a spring to store energy during a flapping cycle [10], [11], [14], [15]. Resonant drives and compliant mechanisms have been implemented in 100mg insect-scale wing flapping mechanisms [1], [2], [5], [18], [23] as well as a 5.8 gram hummingbird-inspired flapping mechanism (pictured in Fig. 1). Recently, Wood [20]–[22] demonstrated lift-off from an insect-scale 60mg flapping-wing MAV, employing a 110Hz wing beat excited at the resonant frequency with a piezoelectric actuator.
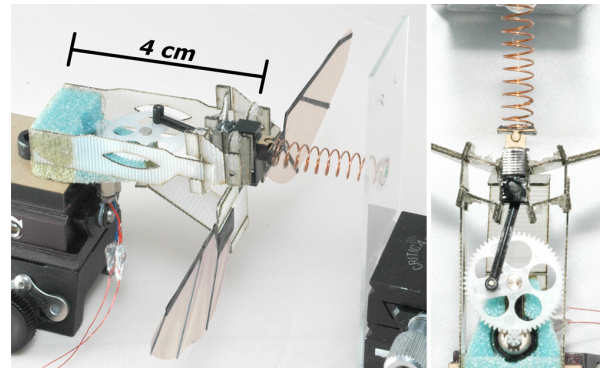

Fig. 1. A 5.8 gram hummingbird-inspired flapping mechanism developed at UC Berkeley.

At the smallest scales, compliant mechanisms, resonant excitation, and piezoelectric actuation work well, due to high speeds, low transmission losses, and high power density. At larger scales, motor actuation is more suitable. Motor-driven, flapping wing MAVs have been built, including the 'Microbat' [8], [16], [17], Kawamura's 2.3 gram MAV [7], the 12 gram Interactive Toys Vamp, and the 'DelFly' [4]. Interestingly, these mechanisms do not explicitly use a resonant drive system. Potentially, resonant excitation can offer increased lift output, with less battery power. However, while analysis of resonant excitation is intrinsically simple for systems driven by piezoelectric actuators (e.g. [5]), it is not straightforward for motor actuated systems. The generation of oscillatory kinematics necessary for flapping-wing flight requires the integration of a crank-arm, which has a fundamental geometric nonlinearity. The integration of compliant mechanisms adds additional nonlinear complexity.

Some of the significant research on the integration of resonant drive mechanisms in DC motor driven flapping wing MAVs is summarized here. Khatait *et al* [12] demonstrated a mechanism that minimized the maximum torque requirement of the DC motor by optimizing the compliant elements of the structure [12]. Tantanawat and Kota [19] proposed integrat-

S. Baek is with the Department of Electrical Engineering and Computer Sciences, University of California, Berkeley, CA 94720, USA `stanbaek@eecs.berkeley.edu`

K. Ma is with the Department of Mechanical Engineering, University of California, Berkeley, CA 94720, USA `kevinma@eecs.berkeley.edu`

R. Fearing is with Faculty of Electrical Engineering and Computer Sciences, University of California, Berkeley, CA 94720, USA `ronf@eecs.berkeley.edu`

ing distributed compliance to reduce the peak input power requirement of the DC motor on a flapping mechanism. Madangopal *et al.* [15], using nonlinear optimization tools, designed a flapping mechanism with springs attached to the load to reduce the variation in motor torque.

Previous work, as cited above, uses peak input power as a design metric. But for mobile battery-powered devices, average input power takes precedence over peak power since average power is directly related to battery capacity. The previous work also assumes the motor is operating at constant velocity, which is difficult to maintain with high loads. Constant input voltage operation, such as from a battery, is more representative of a practical system, rather than assuming constant velocity operation. This is due to the fact that a closed loop speed control requires additional power and components and may require excess peak torques to maintain constant velocity with large load variations.

Here we present a nondimensional analysis of a nonlinear motor-driven crank-arm mechanism coupled to a mass-spring system as a solution to general motor driven oscillators, such as used in flapping flight. Using this analysis, we demonstrate a link between the resonant frequency of a compliant mechanism and the ideal motor input voltage to achieve maximal power reduction. We also demonstrate the effect of the geometric nonlinearity associated with the crank arm and the effect of damping, both motor and aerodynamic. Finally, we apply this analysis to a 5.8g flapping mechanism shown in Fig. 1 and empirically identify the improvement to the system's power plant efficiency.
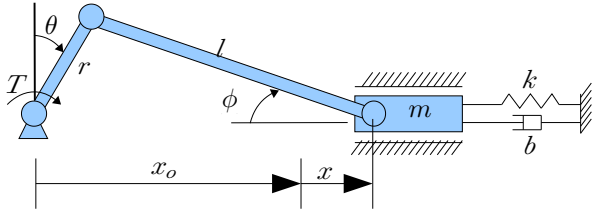
II. ANALYSIS

Fig. 2. A load connected to a spring and a damper is driven by a DC motor through a crank arm.

Compliant mechanisms driven by a DC motor such as the flapping robot pictured in Fig. 1 can be modelled as depicted in Fig. 2. The crank arm driven by a motor/gear is connected to a load (slider) with a spring and a damper. The equation of motion is expressed as:

$$\eta^2 J_m \ddot{\theta} + \eta^2 b_m \dot{\theta} + \frac{r \cos(\phi - \theta)}{\cos(\phi)}(m\ddot{x} + b|\dot{x}|\dot{x} + kx) = T \quad (1)$$

where m is the mass of the load, k is the spring constant, b is the aerodynamic damping coefficient where $b|\dot{x}|\dot{x}$ is the aerodynamic drag force, ϕ and θ are the angular positions of the connecting rod and the crank arm, respectively, l and r are the lengths of the connecting rod and the crank arm, respectively, J_m is the moment of inertia of the motor, b_m

is the damping coefficient of the motor, η is the gear ratio, and T is the torque applied to the crank arm.

The displacement of the slider, x, can be expressed as

$$x = r \sin\theta$$

Substituting x and its derivatives, $\dot{x}$ and $\ddot{x}$, into Eq. (1), we obtain

$$\ddot{\theta}(\eta^2 J_m + \beta mr^2 \cos\theta) + \dot{\theta}\eta^2 b_m + \beta kr^2 \sin\theta$$
$$+ \dot{\theta}^2(\beta br^3 \operatorname{sgn}(\dot{\theta}\cos\theta)\cos^2\theta - \beta mr^2 \sin\theta) = T \quad (2)$$

Here, β is defined as

$$\beta = \frac{\cos(\phi - \theta)}{\cos\phi} = \cos\theta + \frac{\lambda\cos\theta\sin\theta}{\sqrt{1 - \lambda^2\cos^2\theta}}$$

where $\lambda = r/l$ is the ratio of the crank arm length to the connecting rod length. For the second equality, Law of Sines is applied to remove ϕ

$$r\cos\theta = l\sin\phi. \quad (3)$$

The $\operatorname{sgn}(\dot{\theta}\cos\theta)$ term in Eq. (2) can also be simplified to $\operatorname{sgn}(\cos\theta)$ for the direction of motor revolution does not change.

The defining equation of the DC motor is

$$T_m = K_t i \quad (4)$$

$$L\frac{di}{dt} + iR_m + K_e\omega = V_s \quad (5)$$

where V_s is the input voltage, T_m is the torque generated by the DC motor and $T = \eta T_m$, L is the inductance of the motor, i is the induced current, R_m is the resistance, K_e is the back EMF coefficient, and K_t is the torque coefficient of the motor. Since L is generally very small, we can safely set $L = 0$ for the rest of the analysis in this paper. Substituting Eq. (4) and Eq. (5) into Eq. (2), we can obtain the equation of the overall dynamic system:

$$\ddot{\theta}(\eta^2 J_m + \beta mr^2 \cos\theta) + \dot{\theta}\eta^2\left(b_m + \frac{K_t K_e}{R_m}\right) + \beta kr^2 \sin\theta$$

$$+ \dot{\theta}^2(\beta br^3 \operatorname{sgn}(\cos\theta)\cos^2\theta - \beta mr^2 \sin\theta) = \frac{\eta K_t}{R_m}V_s \quad (6)$$

To obtain a nondimensional equation of motion, define the following variables:

$$
\begin{array}{ll}
\omega_n = \sqrt{k/m} & \tau = \omega_n t \\
\Omega = d\theta/d\tau = \dot{\theta}/\omega_n & \dot{\Omega} = d^2\theta/d\tau^2 = \ddot{\theta}/\omega_n^2 \\
J = \eta^2 J_m/mr^2 & B_m = b_m + K_t K_e/R_m \\
\zeta = br/(2m) & \zeta_m = \eta^2 B_m/(2mr^2\omega_n) \\
\tilde{T} = T/(mr^2\omega_n^2) &
\end{array}
$$

Here, ω_n is the undamped natural frequency of the mass-spring system of the slider, τ is the nondimensional time, ζ and ζ_m are the damping ratios of the slider and the damping ratio of the motor, respectively, Ω and $\dot{\Omega}$ are, respectively, the nondimensional angular velocity and angular acceleration of the motor, J is the nondimensional moment of inertia, B_m

is the effective motor damping, and $\tilde{T}$ is the nondimensional motor torque.

We can now obtain a nondimensional equation of motion for Eq. (6) as follows

$$(J + \beta\cos\theta)\dot{\Omega} + 2\zeta_m\Omega + \beta\sin\theta$$
$$+ (2\zeta\beta\,\mathrm{sgn}(\cos\theta)\cos^2\theta - \beta\sin\theta)\Omega^2 = u \quad (7)$$

where u is the nondimensional input voltage defined as

$$u = \frac{\eta K_t}{mr^2 R_m \omega_n^2} V_s$$

With $\dot{\Omega} = 0$ for the case of constant motor speed, Eq. (7) becomes

$$2\zeta_m\Omega + \beta\sin\theta$$
$$+ (2\zeta\beta\,\mathrm{sgn}(\cos\theta)\cos^2\theta - \beta\sin\theta)\Omega^2 = u \quad (8)$$

A. Case I: Constant Speed

It is rather easy to understand the behavior of the resonant drive with a constant speed excitation due to the similarity to linear mass-spring systems. The variation of torque required to drive the system in one cycle is shown in Fig. 3 (top). The peak value of the output torque becomes minimal close to $\Omega = 1.0$, where the system is excited at its resonant frequency. This plot agrees with the results of the minimal torque approach studied by Khatait *et al.* [12]. In their study, they have demonstrated that there is a certain value of torsional stiffness of flexural joints corresponding to the driving frequency that minimizes the peak input torque. Indeed, the corresponding driving frequency in their study is fundamentally identical to the resonant frequency of the compliant system discussed here. Additionally, the choice of spring constant in the study of Tantanawat and Kota [19] indeed provides their compliant system with the resonant frequency matching with the desired flapping frequency so that the peak input power is minimized.

It should also be noted that for the values of Ω away from 1, negative torques are required to drive the system at a constant speed, i.e., excessive kinetic energy of the inertial load is transmitted back to the motor instead of converted to strain energy in the spring. Tantanawat and Kota have assumed in their study that this negative input power, which is the energy absorbed by the motor from the load, is fully recovered. However, this is not true when taking into account motor and battery resistance - power is still dissipated with negative current on the resistors. From a controls standpoint, absorbing the energy for later use or supplying negative current to decelerate the plant is undesirable.

In fact, the variation of input torque can also be reduced tremendously by reducing the ratio of the crank arm length to the connecting rod length, λ. As shown in Fig. 3 (bottom), the peak input torque becomes smaller as λ decreases. The torque variation also becomes more symmetrical, and negative input torque is no longer required.[1] However, an

excessively small value of λ (very long connecting rod) results in undesirable bending modes of the connecting rod. $\lambda \geq 0.2$ is also undesirable because it requires not only high peak torques but also negative torques to keep the speed constant.
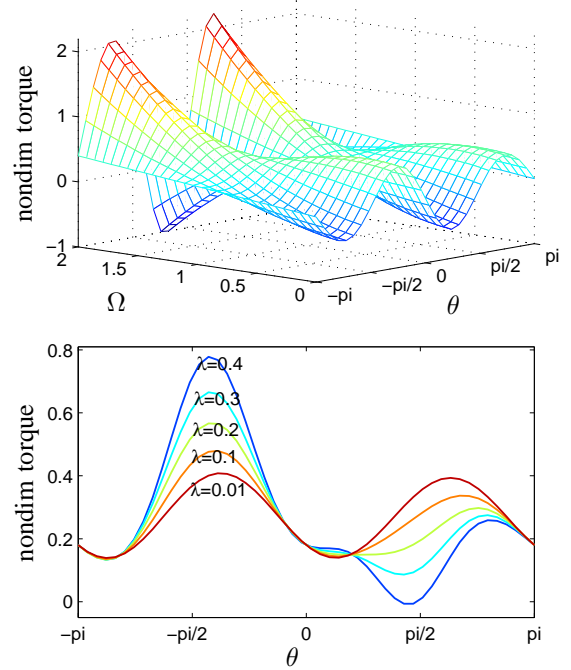

Fig. 3. Variation of nondimensional torque in one cycle for various constant angular speed with $\lambda = 0.1$, $\zeta_m = 0.1$, and $\zeta = 0.1$ (top). Variation of nondimensional torque in one cycle for various values of λ with $\Omega = 0.9$, $\zeta_m = 0.1$, and $\zeta = 0.1$ (bottom).

Nondimensionalized average power required to drive the system in one cycle for various damping ratio is shown in Fig 4. The average power is reduced at $\Omega \sim 1$ when $\zeta \leq 0.2$, i.e., at $\Omega \sim 1$ we can achieve a local minimum of the power to drive the crank.[2] As the damping ratio increases, an addition of a spring to the system makes a negative contribution because the input power supplies not only the energy dissipated in the damper but also the energy to be stored in the spring.

B. Case II: Constant Input Voltage

When a constant voltage is applied to the DC motor, the resonant drive behavior becomes more complicated since the frequency of the applied force (or the motor speed) to a load no longer remains constant. The motor speed and torque, however, stay almost constant if the system is driven at its resonant frequency and the damping ratio is small ($\zeta_m = 0.02$ and $\zeta = 0.01$) as shown in Fig. 5. It is apparent that the peak input power becomes minimal when

---

[1]Indeed, with $\lambda \sim 0$, ϕ becomes 0 and the force applied to the mass through the connecting rod becomes a pure sinusoidal input to the mass-spring system.

[2]The global minimum occurs at $\Omega = 0$, but $\Omega \sim 0$ is not an interesting region.
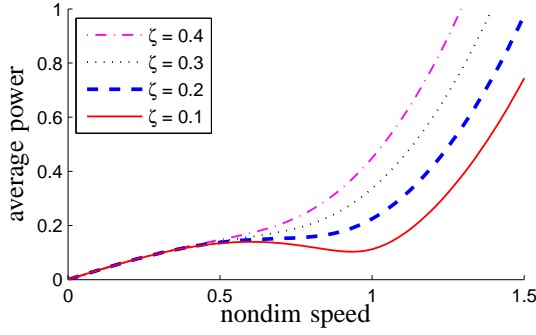
Fig. 4. Nondimensional average power required to drive the system at a constant angular speed for various damping ratios with $\lambda = 0.1$, $\zeta_m = 0$

the nondimensional input voltage u is 0.25.[3] As the input voltage increases or decreases, the torque becomes more oscillatory and eventually becomes negative, i.e., some of the kinetic energy of the load is transmitted back to the battery instead of stored in the spring.
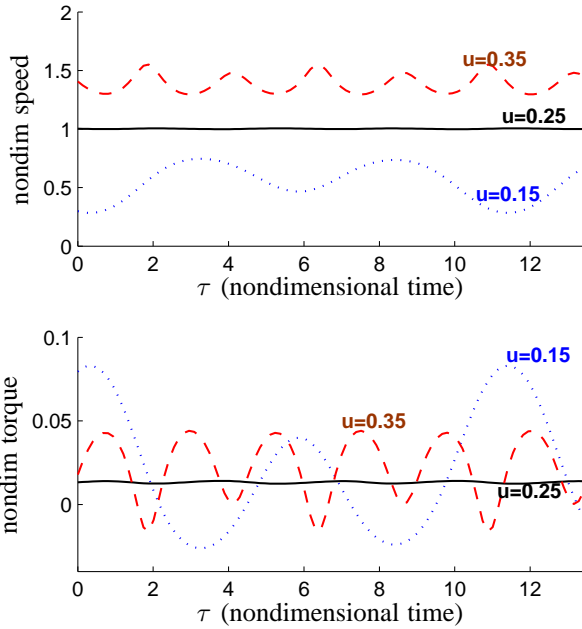

Fig. 5. Variation of nondimensional speed (top) and torque (bottom) for various nondimensional input voltages ($\zeta_m = 0.02$ and $\zeta = 0.01$)

The effect of the aerodynamic damping ratio ζ is shown in Fig. 6. As the damping ratio increases, the required torque to drive the load clearly increases while the motor speed decreases. Both torque and motor speed become more oscillatory, which can be expected from the $\zeta\beta\cos^2\theta$ term in Eq. (7). The effect of ζ_m is, however, independent of the

<hr>

[3]It should be noted that the induced motor current is directly proportional to the motor torque as presented in Eq. (4). Hence, the electrical power for the motor as well as the mechanical power from the motor have the minimal peak-to-peak values.

oscillating behaviors as expected from the $2\zeta_m\Omega$ term, and the DC value of Ω monotonically decreases as ζ_m increases. The effect of the parameter ζ_m is basically the same as a damping ratio of a linear mass-spring-damper system. As a side note, this model also provides an estimate of motor velocity for a given battery voltage, for which no closed-form solution is available.
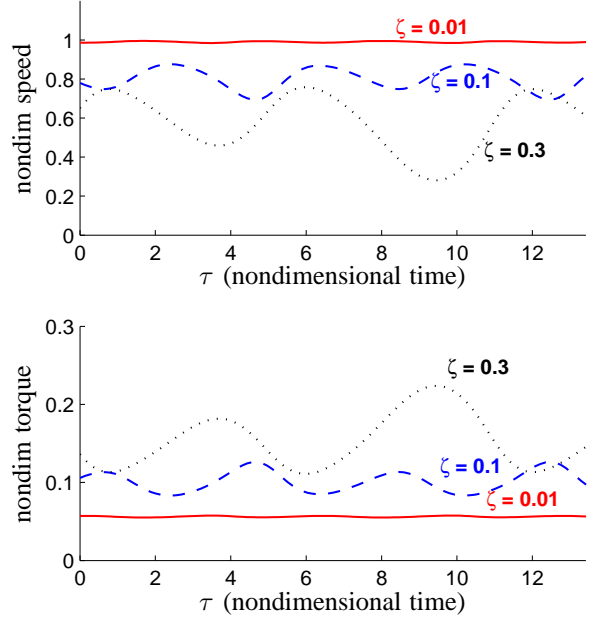

Fig. 6. Variation of nondimensional speed (top) and torque (bottom) for various damping ratios, ζ, ($\zeta_m = 0.02$ and $u = 0.25$).

The required average input power with respect to the mean of nondimesional motor speed, E[Ω], is shown in Fig. 7.[4] While the average power with no spring monotonically increases with the speed, the average power with a spring has a minimum. The best improvement of efficiency occurs when E[Ω] is approximately 1. It is well known that the magnitude response for a linear mass-spring system becomes less than unity with an out-of-phase drive and therefore no power benefits can be achieved when compared to a spring-less system. However, power reduction can be achieved for the motor driven compliant system studied here even though the operating speed is significantly higher than the undamped natural frequency of the load. The significant prediction is that low damped mechanical systems with a spring driven by a DC motor can be excited at a higher speed than the system without a spring for the same amount of input power. Hence, greater power can be obtained or a smaller motor can be used.

<hr>

[4]Data is not available for E[Ω] < 0.5 because small values of constant input voltage cannot overcome the initial spring force to complete a revolution.
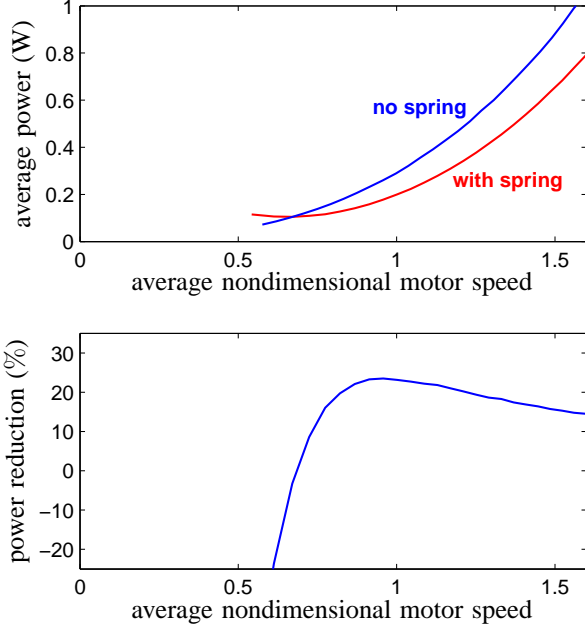
Fig. 7. average power (top) and power reduction using a spring (bottom) with respect to the mean of nondimensional motor speed E[Ω]. ($\zeta_n = 0.02$ and $\zeta = 0.05$)
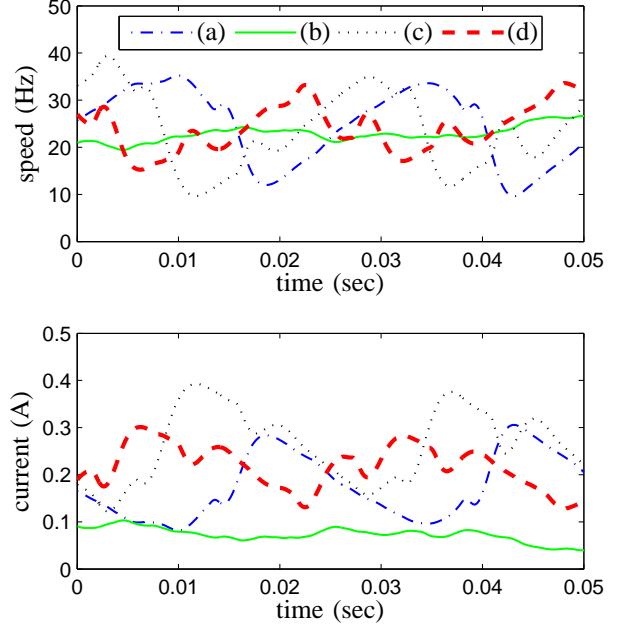

Fig. 8. Measurement of motor speed with constant input voltage (top) and measurement of induced current with constant input voltage(bottom). (a) no spring in vacuum at V = 1.45V (b) with spring in vacuum at V = 1.05V (c) no spring in air at V = 1.70V (d) with spring in air at V = 1.55V.

III. EXPERIMENTS

The flapping mechanism shown in Fig. 1 consists of two mirrored levers actuated by a single DC motor. The fulcrum of each lever is cantilevered by a beam and hinge from a base structure that also houses the DC motor coupled to a gearbox and crank. Due to the kinematic constraints set by the equal lengths of both fulcrum beams, the system effectively becomes a slider-crank mechanism. Motion normal to the lever plane is restricted by the geometry of the fulcrum beams, and an additional Sarrus linkage, positioned between the driving block and the base structure and operating out of plane, effectively constrains the motion of the driving block along the intended linear path. The specifications of the flapping mechanism are given in Table I.

TABLE I
SPECIFICATIONS OF THE FLAPPING MECHANISM

motor inertia	1.41gm-mm^2
motor damping	8.26gm-mm^2/s
gear ratio	1:8.57
wing inertia	142.9gm-mm^2
air damping	0.05-0.11kg/m for $\dot{\theta}$=120-160s^{-1}
spring constant	140N/m
crank arm	4 mm
connecting rod	17 mm
total mass	5.8 gm

The motor velocity and the measured current of the flapping mechanism with and without a linear coiled spring

were measured as shown in Fig. 8. The additional 140N/m spring was added between the slider crank and the ground. The undamped natural frequency of the load was calculated as $\omega_n = 155$rad/s (24.5Hz) with the effective wing mass of 5.83×10^{-3}kg.[5] Measurements were also taken in vacuum in order to verify our analysis for the crank-arm model with extremely low aerodynamic damping. With the measurements in vacuum, we could examine the aerodynamic damping versus internal damping of the mechanism. The motor damping ratio and aerodynamic damping ratio are calculated to be $\zeta_m = 0.13$ and $\zeta = 0.03$, respectively.[6] For the same mean motor speed of 24Hz, the speed variation as well as current variation for the mechanism with a spring are smaller than those without a spring both in air and in vacuum. The RMS current (and torque) is also lower with a spring than without a spring, which implies that lower mechanical power is required with a spring to generate the same flapping frequency.

The average power and power reduction for various flapping frequencies are shown in Fig. 9. At high input voltages where the average motor speeds were greater than 15Hz, the average power for the system with spring became less than the system without spring. With extremely low aerodynamic

[5]The effective mass of the wings were calculated as $m_w = 2J_w/d^2$, where J_w is the moment inertia of a single wing and d is the distance between the fulcrum and the pin joint coupling the connecting rod and the lever arm.
[6]To calculate the aerodynamic damping, we measured motor velocity and current for the flapping mechanism in vacuum as well as in air. Using these measurements, we estimated the damping coefficient, b.
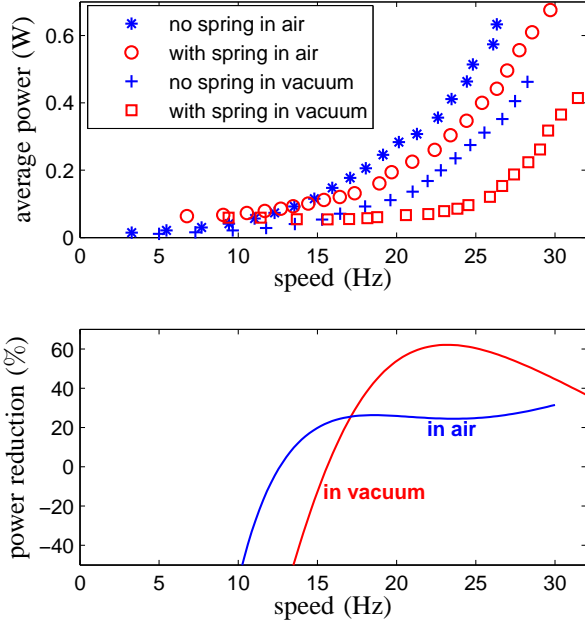
Fig. 9.   Measurement of average power (top) and power reduction using a spring (bottom) for a flapping wing robot driven by constant input voltages

damping in vacuum, we could achieve up to 60% power reduction. We also achieved up to 30% power reduction when flapping at 15-30Hz with a constant input voltage of 1-3V DC. This can increase continuous flight time and decrease battery mass. The percent power reduction remained almost constant as the flapping frequency increases.

We briefly examined the effect of an integrated spring on the lift force generated by our flapping mechanism. Our results showed a 20-30% increase in average lift force for the spring-integrated system, relative to the spring-less system operating at the same flapping frequency. The electrical input power was also reduced, as predicted. Hi-speed video showed a more symmetric upstroke and downstroke in the spring-integrated system. The experiment indicates that the spring, in addition to reducing input power at a given operating frequency, is also beneficially altering the flapping wing trajectory. This result essentially agrees with the study by Khan *et al* [9] in that appropriate spring constant and inertia can increase the lift force with less input power. In their study, the spring constant and inertia were chosen by numerical optimization.

We also modified an Interactive Toy's VAMP RC ornithopter by adding a 980N/m spring as shown in Fig. 10 to briefly verify our crank-arm model analysis on another system. The ornithopter flaps at 14-16Hz with a fully charged 40mAh lithium polymer battery. On-board electronics, battery, and styrofoam outfit were removed from the ornithopter, and the motor was directly connected to a power supply. The undamped natural frequency of the load was calculated as $\omega_n = 118.4$rad/s (18.8Hz) with the effective wing mass

of 69.85×10^{-3}kg. Measurements were also taken without a spring to compare the power consumption.
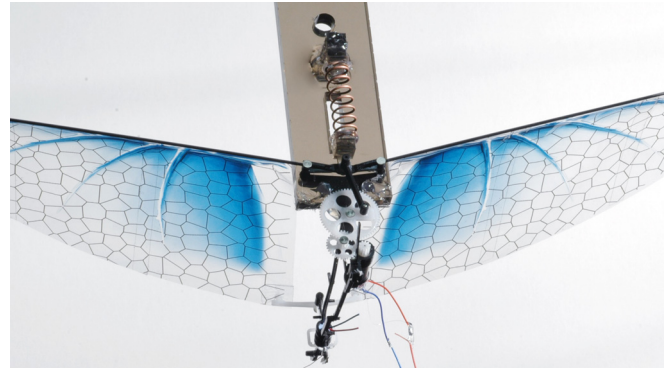

Fig. 10.   An Interactive Toy's VAMP RC ornithopter with an added spring

Shown in Fig. 11 are the average power and power reduction for various flapping speeds. When the average motor speed was greater than 12Hz, the average power for the system with spring became less than for the system without spring. We have achieved up to 19% power reduction at 16Hz. It would be possible to obtain a similar amount of power reduction even at higher flapping frequencies if the motor could operate at higher input voltages.
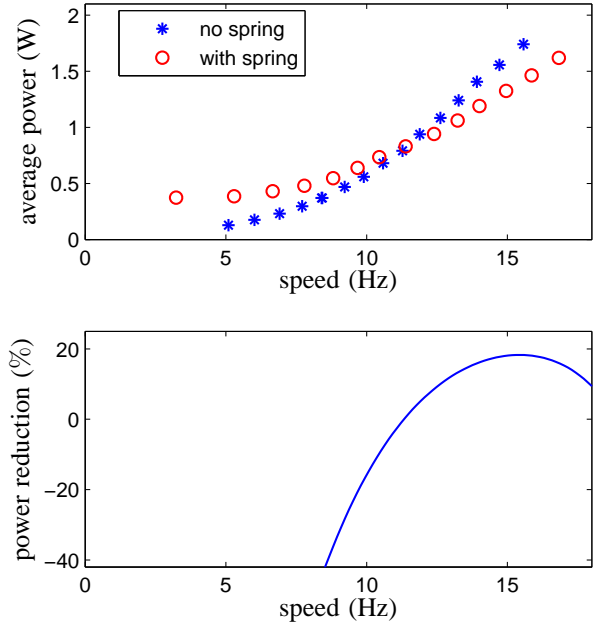

Fig. 11.   Measurement of average power (top) and power reduction using a spring (bottom) for an Interactive Toy's VAMP RC ornithopter

IV. CONCLUSION

In this paper, we have shown that battery and motor resistance plays an important role in the efficiency of power

transmission to the environment for a resonant flapping-wing mechanism. With a nondimensional analysis of a motor driven compliant system, we have analytically developed a methodology to guide the mechanical design and predict optimal operating points based on power efficiency. We have also experimentally demonstrated that the average power (as well as the peak torque) can be reduced by resonant excitation with a constant voltage for motor-driven oscillating systems. Moreover, simulations show that an average power of 0.43W with 0.13W peak-to-peak is required to drive a crank-arm system at the average speed of 150rad/sec (s.d. = 7.7rad/sec) with a constant voltage of 2.65V, while an average power of 0.48W with 0.22W peak-to-peak (not including the power for speed controller) is required for the constant speed of 150rad/sec.[7] In addition to this specific example, the generalized crank-arm model presented in this paper can be easily applied to most motor-driven oscillating systems by constructing an equivalent crank-arm model.

REFERENCES

[1] S. Avadhanula, R. Wood, D. Campolo, and R. Fearing, "Dynamically tuned design of the MFI thorax," in *IEEE Int. Conf. on Robotics and Automation*, Washington, DC, May 2002.

[2] S. Avadhanula, R. Wood, E. Steltz, J. Yan, and R. Fearing, "Lift force improvements for the micromechanical flying insect," in *IEEE/RSJ Int. Conf. on Intelligent Robots and Systems*, October 2003.

[3] A. Cox, D. Monopoli, D. Cveticanin, M. Goldfarb, and E. Garcia, "The development of elastodynamic components for piezoelectrically actuated flapping micro-air vehicles," *Journal of Intelligent Material Systems and Structures*, vol. 13, pp. 611–615, September 2002.

[4] (2009) Delfly. Delft University of Technology. The Netherlands. [Online]. Available: http://www.delfly.nl/

[5] R. Fearing, K. Chiang, M. Dickinson, D. Pick, M. Sitti, and J. Yan, "Wing transmission for a micromechanical flying insect," in *IEEE Int. Conf. on Robotics and Automation (ICRA)*, April 2000.

[6] G. Fischer, A. G. Cox, M. Gogola, M. K. Gordon, N. Lobontiu, D. Monopoli, E. Garcia, and M. Goldfarb, "Elastodynamic locomotion in mesoscale robotic insects," in *SPIE conference on Electroactive Polymer Actuators and Devices*, vol. 3669, March 1999, pp. 362–368.

[7] Y. Kawamura, S. Souda, S. Nishimotor, and C. Ellington, *Bio-mechanisms of Swimming and Flying: Fluid Dynamics, Biomimetic Robot, and Sports Science*. Springer, 2008, ch. 26: Clapping-wing Micro Air Vehicle of Insect Size, pp. 319–330.

[8] M. Keennon and J. Grasmeyer, "Development of the Black Widow and Microbat MAVs and a vision of the future of MAV design," in *AIAA International Air and Space Symposium and Exposition: The Next 100 Years*, Dayton, Ohio, July 2003.

[9] Z. Khan, K. Steelman, and S. Agrawal, "Development of insect thorax based flapping mechanism," in *IEEE International Conference on Robotics and Automation*, Kobe, Japan, May 2009.

[10] Z. A. Khan and S. K. Agrawal, "Design of flapping mechanisms based on transverse bending phenomena in insects," in *IEEE International Conference on Robotics and Automation*, Orlando, FL, May 2006.

[11] ——, "Design and optimization of a biologically inspired flapping mechanism for flapping wing micro air vehicles," in *IEEE International Conference on Robotics and Automation*, Rome, Italy, April 2007.

[12] J. P. Khatait, S. Mukherjee, and B. Seth, "Compliant design for flapping mechanism: A minimum torque approach," *Mechanism and Machine Theory*, vol. 41, pp. 3–16, 2006.

[13] N. O. Lobontiu, M. K. Gordon, G. Fischer, E. Garcia, and M. Goldfarb, "Design and analysis of elastodynamic locomotion for robotic insects," in *SPIE conference on Microrobotics and Micromanipulation*, vol. 3519, November 1998, pp. 118–127.

[14] R. Madangopal, Z. Khan, and S. K. Agrawal, "Energetics-based design of small flapping-wing micro air vehicles," *IEEE/ASME Transactions on Mechatronics*, vol. 11, no. 4, p. 433, August 2006.

[15] R. Madangopal, Z. A. Khan, and S. K. Agrawal, "Biologically inspired design of small flapping wing air vehicles using four-bar mechanism and quasi-steady aerodynamics," *ASME Journal of Mechanical Design*, vol. 127, pp. 809–816, July 2005.

[16] T. N. Pornsin-Sirirak, S. W. Lee, H. Nassef, J. Grasmeyer, Y. Tai, C. Ho, and M. Keennon, "MEMS wing technology for a battery powered ornithopter," in *The 13th IEEE Annual International Conference on MEMS*, 2000, pp. 709–804.

[17] T. Pornsin-Siririak, Y. Tai, H. Nassef, and C. Ho, "Titanium-alloy MEMS wing technology for a micro aerial vehicle application," *Journal of Sensors and Actuators A: Physical*, vol. 89, pp. 95–103, March 2001.

[18] E. Steltz, S. Avadhanula, and R. Fearing, "High lift force with 275 Hz wing beat in MFI," in *IEEE/RSJ International Conference on Intelligent Robots and Systems*, San Diego, CA, 2007.

[19] T. Tantanawat and S. Kota, "Design of compliant mechanisms for minimizing input power in dynamic applications," *ASME Journal of Mechanical Design*, vol. 129, pp. 1064–1075, October 2007.

[20] R. J. Wood, "Design, fabrication, and analysis of a 3DOF, 3cm flapping-wing MAV," in *IEEE/RSJ International Conference on Intelligent Robots and Systems*, San Diego, CA, 2007.

[21] ——, "Liftoff of a 60mg flapping-wing MAV," in *IEEE/RSJ International Conference on Intelligent Robots and Systems*, San Diego, CA, 2007.

[22] ——, "The first takeoff of a biologically inspired at-scale robotic insect," *IEEE Trans. Robotics*, vol. 24, no. 2, pp. 341–347, 2008.

[23] J. Yan, R. Wood, S. Avadhanula, M. Sitti, and R. Fearing, "Towards flapping wing control for a micromechanical flying insect," in *IEEE Int. Conf. on Robotics and Automation*, Seoul, Korea, 2001, pp. 253–262.

---

[7] The specifications of the system in the simulations are: $\eta=8.6$, $\zeta_n = 0.1$, $\zeta = 0.01$, $\lambda = 0.2$, $K_t = 0.2$Nmm/A, $K_e = 0.67$mV-sec, and $J_m = 1.4$gmm^2.